A Super-Wideband Miniaturized Graphene-Based Folded Monopole Antenna

Li Guo
School of Automation and Electronic Information, Xiangtan University, Xiangtan, China
Corresponding author: Li Guo (e-mail: guoli_31@xtu.edu.cn)

ABSTRACT A graphene-based folded monopole antenna with super-wideband bandwidth and a small volume is proposed in this paper. The antenna features a disc-loaded folded cylindrical configuration that mainly consists of graphene-powder and graphene-ink cylinders, along with copper discs. Two primary radiation modes are generated and combined to achieve the desired super-wideband bandwidth. The applied graphene-powder and graphene-ink cylinders serve as crucial radiating and tunable elements, rendering the antenna impedance matched across the super-wideband range. Furthermore, direct current (DC) excitation combined with conducting wires is utilized to improve impedance matching and enhance the operating bandwidth toward lower frequencies. The measured results indicate that the antenna has a super-wideband operating bandwidth across 0.114-0.202 GHz and 0.34-18 GHz ($|S_{11}|$ <-6 dB). The measured antenna peak gains range from -3.75-3.50 dBi. The antenna dimensions can be maintained at $0.006\lambda_L \times 0.006\lambda_L \times 0.011\lambda_L$, where λ_L is the wavelength in free space at the lowest operating frequency.

INDEX TERMS Super-wideband, graphene, monopole antenna, miniaturization.

I. INTRODUCTION

WITH the advancement of wireless technologies, one of the primary challenges in antenna design is overcoming the fundamental limitations of antennas [1]. The trade-off between antenna bandwidth and electrical size is a significant challenge, particularly when it comes to miniaturized super-wideband antennas [2]. Several problems need to be addressed, particularly regarding super-wideband impedance matching and bandwidth enhancement. One promising method is utilizing graphene-based composites and structures for developing such antennas [3]. However, the use of graphene-based materials, for example, a dielectric or conductor made from multilayer graphene, as components in antennas that serve as both resonant and radiating elements is a promising area for exploration [4]–[6]. This is partly due to advancements in fabrication techniques, which enable the production of various types of graphene materials that possess unique properties and characteristics. These include conductivity-based properties, tunable characteristics, and frequency-dependent behavior [7], [8]. Additionally, graphene-based materials are often used in combination with metals to design antennas [9]. The contact impedance between metal and graphene can vary across a wide range of frequencies, which could be utilized for nonlinear conductivity-based impedance matching or dynamic control for enhanced super-wideband bandwidth [10], [11].

To achieve simultaneous super-wideband performance and miniaturization in antenna design, several innovative approaches can be utilized. These include the use of dielectric resonators/material [12], [13], fractal structures [14], active/passive components, and geometry-independent concepts [15]. When using certain graphene-based materials as the radiating element in antenna designs at the microwave band, it encounters challenges such as the high surface resistance of graphene compared to metals, the electrical size needing to satisfy the order of the wavelength, and low radiation efficiency [5], [16]. Additionally, some graphene-based components may not be self-resonant when integrated into antennas because of their relatively high resistance [16], [17]. Therefore, multilayer graphene and hybrid metal-graphene antenna configurations, which combine graphene with traditional metal materials such as copper, are employed to leverage the frequency-dependent, tunable, and conductivity-based properties of graphene [7], [18]. This approach holds significant promise for achieving impedance matching over a super-wideband range [19], offering an effective solution for expanding bandwidth and enhancing antenna performance, particularly at the microwave band [7]. Accordingly, several types of graphene samples or forms are particularly suited for microwave antenna designs and fabrication, such as few-layer graphene (FLG) [20], multilayer graphene films (MGF), multilayer chemical vapor deposition (CVD) graphenes [10], nanographene particles, and graphene inks [21]. Although graphene powder is less commonly used,

suspended graphene can create high-conductivity composites and offer tunable properties for flexible designs [22]. Generally, when graphene is doped, it exhibits a non-linear conductivity response. Notably, embedding conducting wires for DC bias is a practical method of doping graphene in a fabricated graphene-based antenna [23]. The disc-loaded folded cylinder structure is a well-known design in antenna engineering. It typically involves a cylindrical antenna element that is folded and loaded with discs, which can be effectively applied to construct graphene-based antennas with a monopole-like radiation pattern [24].

In this paper, a super-wideband miniaturized graphene-based monopole antenna is proposed. The antenna features a hybrid copper-graphene disc-loaded folded cylindrical configuration and incorporates multilayer nanographene. The antenna was constructed and simulated using CST Microwave Studio. Subsequently, it was fabricated and measured. Deep insights into its working principle have been explored and analyzed. The performance parameters of the antenna were analyzed and contrasted. A conclusion is provided at the end.

II. DESIGN OF MINIATURIZED SUPER-WIDEBAND GRAPHENE-BASED FOLDED MONOPOLE ANTENNA

A. ANTENNA CONFIGURATION

The configuration of the proposed super-wideband miniaturized graphene-based folded monopole antenna is presented in Fig. 1. As can be seen, the antenna consists of a top-hat copper disc, a circular ground plane, a cylindrical monopole, a graphene-powder cylinder that surrounds the outside surface of the cylindrical monopole, and two graphene-ink cylinders that are shorted between the top-hat copper disc and the circular ground plane. In the simulation, the graphene-powder and the graphene-ink cylinders are modeled by creating new materials in CST. The conductivities and the relative dielectric constants of the created graphene-powder and graphene-ink materials,made from multilayer nanographene, are set within a range of 100000-1000000 S/m and 1-1000 for different frequencies in CST [25], [26]. Notably, the applied multilayer graphene materials are set to anisotropic. Adaptive mesh refinement is applied to simulate the antenna in CST. The conductivities and dielectric constants change at different frequencies to model the non-linear frequency-dependent characteristics of the graphene-powder and –ink materials, which contribute to the generated super-wideband bandwidth. Three plastic PVC tubes are used to encapsulate the graphene-ink cylinders and the graphene-powder cylinder. The antenna is also fed by an SMA coaxial probe from below. The entire antenna configuration resembles a hurricane lamp. Three 12-V DC voltage sources are connected at excitation point 1, 2, and 3, which are located between the cylindrical monopole and the top-hat copper disc and between the graphene-powder cylinder and the graphene-ink cylinders, respectively. This excitation voltage value was determined through practical testing experiments, demonstrating that the available graphene samples have better conductivity with 12-V DC excitation.

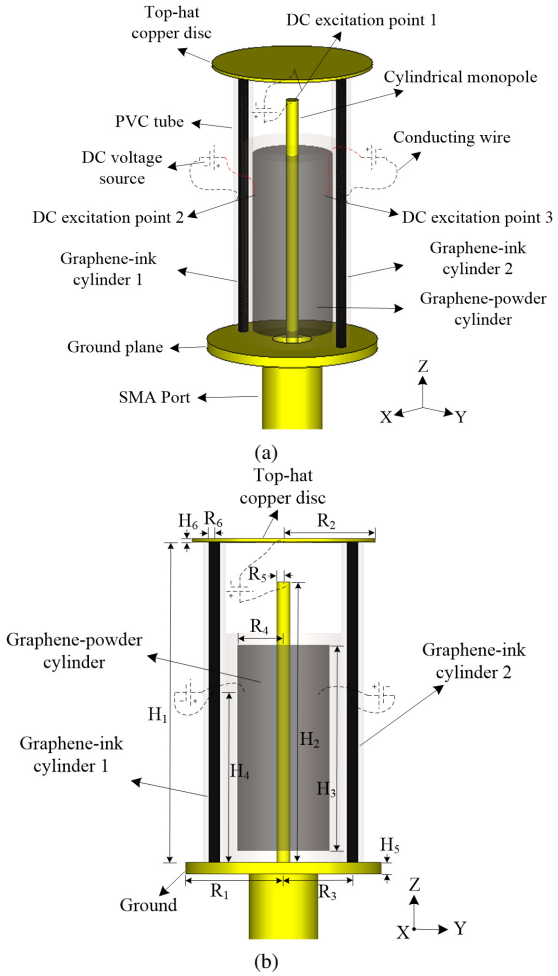

FIGURE 1: Configuration of the proposed antenna. (a) 3D view, (b) side view. The labeled dimensions are: H_1=28 mm, H_2=25 mm, H_3=18 mm, H_4=15 mm, H_5=1 mm, H_6=0.3 mm, R_1=8.5 mm, R_2=8 mm, R_3=6 mm, R_4=4 mm, R_5=0.6 mm, R_6=0.5 mm.

B. RADIATION MODES

Investigation into the working principle of the proposed antenna was conducted. The radiation modes are first extracted as depicted in Fig. 2. There are two primary frequency-independent radiation modes, namely mode #1 and mode #2, which combine to generate the enhanced super-wideband bandwidth with a monopole-like radiation pattern [27]. Mode #1 operates in the lower band (<10 GHz) while mode #2 operates in the higher band (>10 GHz) [28]. Notably, for the lower band, the DC voltage excitation contributes to the enhanced super-wideband bandwidth. The corresponding vector current distributions of both modes are depicted in Fig. 2. As can be seen, mode #1 exhibits two common-center folded monopole modes with fixed radiating paths across the lower band, taking advantage of reduced dimensions and enhanced radiation. Meanwhile, mode #2 exhibits two common-center folded monopole modes but with a truncated radiating path relative to mode #1 and a variable radiat-

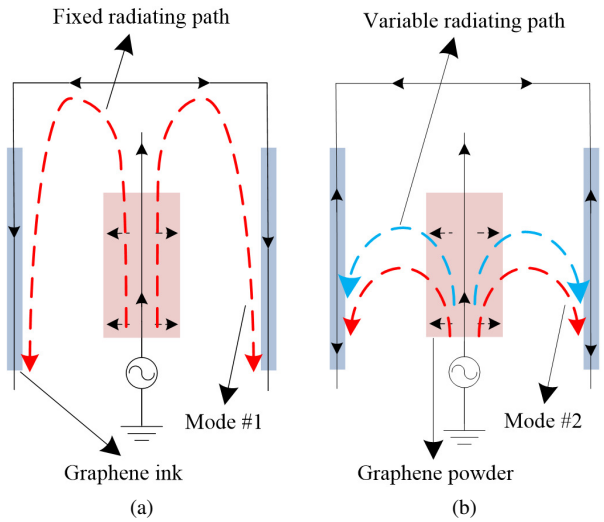

FIGURE 2: Radiation modes of the proposed antenna: (a) mode #1 for the lower band (<10 GHz), (b) mode #2 for the higher band (>10 GHz).

ing path with frequency. The radiation of mode #2 mainly originates from the graphene-powder cylinder with tunable non-linear frequency-dependent conductivity. On the other hand, the tunable conductivity of the graphene-ink cylinders serves as the primary function for the frequency-independent radiation of mode #1. From another perspective, modes #1 and #2 can be regarded as hybrid modes that are composites of the $HE_{11\delta}$ mode, the folded monopole mode, and the $HE_{11\delta}$ mode [29].

C. EQUIVALENT CIRCUIT AND CONDUCTIVITY-BASED PROPERTIES

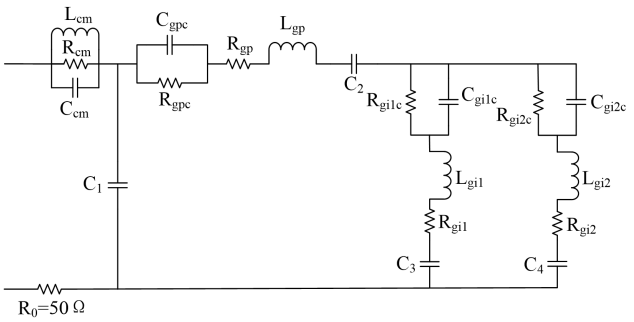

FIGURE 3: Equivalent circuit of the proposed antenna.

In terms of the proposed antenna configuration, the corresponding equivalent circuit is identified as shown in Fig. 3. The contact resistances (R_{gpc}, R_{gi1c}, and R_{gi2c}) and the contact capacitances (C_{gpc}, C_{gi1c}, and C_{gi2c}) are the equivalent lumped components at the interface of the cylindrical monopole and the graphene-powder cylinder, and at the interface of the top-hat copper disc and the graphene-ink cylinders, which play a critical role in the conductivity-based properties [24]. Particularly, in the lower band, the contact resistances dominate the antenna operation, and the currents flow mainly through the contact resistances. In contrast, in the higher band, the contact capacitances dominate. By increasing the carrier density in the graphene, a higher contact capacitance can be achieved, resulting in higher conductivity and improved radiation efficiency [10]. This can be implemented through various approaches, such as doping graphene and applying DC voltage excitation. Additionally, as the conductivity increases, more efficient carrier injection from metal to the multilayer graphene can be realized. The intrinsic resistance R_{gp} of the graphene-powder cylinder and the inductance L_{gp} arise from the properties of the graphene-powder material. C_2 is the coupling capacitance between the cylindrical monopole and the top-hat copper disc. C_3 and C_4 are the gap capacitances between the graphene-powder cylinder and the graphene-ink cylinders 1 and 2, respectively. L_{cm}, R_{cm}, and C_{cm} are the equivalent inductance, resistance, and capacitance of the cylindrical monopole, respectively. C_1 is a capacitance that separates the cylindrical monopole from the graphene-powder cylinder. It should be noted that the values of the lumped components in the equivalent circuit change with different operating states of modes #1 and #2.

A number of factors affect the conductivity of the included graphene-based cylinders in the proposed antenna. In general, the total conductivity is denoted as $\bar{\bar{\sigma}}_T(\omega)$. The antenna input impedance is inversely related to the total conductivity of the graphene-based cylinders, and this is expressed by formula 1 [30].

$$Z_{in} = R_{in} + jX_{in} \propto \frac{1}{J} = \frac{1}{\bar{\bar{\sigma}}_T(\omega)\overrightarrow{E}} \tag{1}$$

where $\overrightarrow{E}$ is the vector E-field on the graphene-based cylinders surface. In terms of formula 1, the input impedance of the antenna can be adjusted by tuning the conductivity.

D. INPUT IMPEDANCE PROPERTIES OF THE PROPOSED ANTENNA

The effect of varying the proposed antenna dimensions on the input impedance properties was investigated. Firstly, the height of the top-hat copper disc is changed by varying the height of the two graphene-ink cylinders. The curves for the real and imaginary parts of the antenna's input impedance are depicted in Fig. 4.

By increasing the height of the top-hat copper disc, it can be observed that the impedance matching becomes worse. When reducing the height, although better impedance properties can be achieved, the distance between the top-hat copper disc and the cylindrical monopole decreases, which complicates the assembly and soldering of the conducting wires during the fabrication process.

The radius of the graphene-ink cylinders affects the contact area between the copper and the graphene. This, in turn, influences the component values in the equivalent circuit, including the contact resistances C_{gi1c} and C_{gi2c}, as well as the

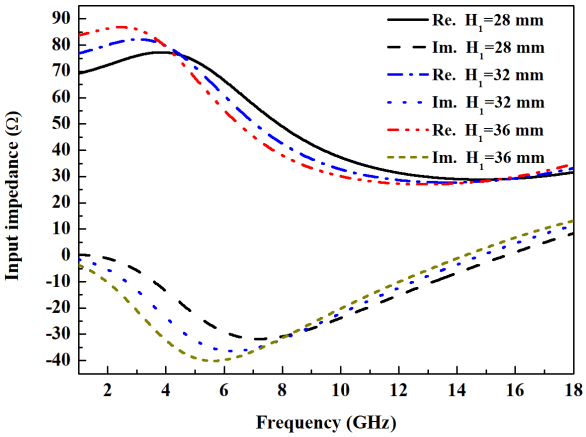

FIGURE 4: Effect of varying the height of the top-hat copper disc on the antenna input impedance.

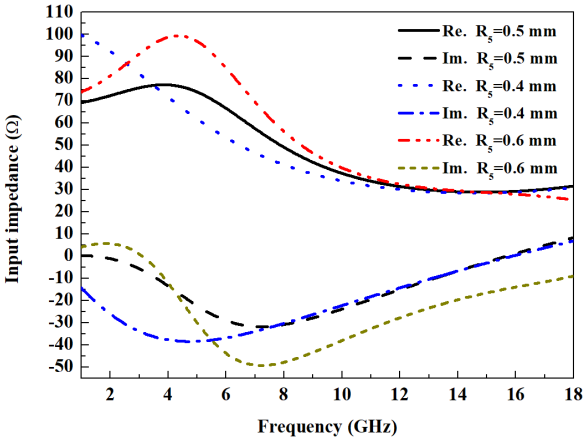

FIGURE 5: Effect of varying the radius of the graphene-ink cylinders on the antenna input impedance.

contact capacitances C_{gi1c} and C_{gi2c}. The effect of varying this radius on the antenna input impedance (specifically its real and imaginary parts) is simulated and depicted in Fig. 5. Additionally, the radius of the graphene-powder cylinder also influences the antenna input impedance. The corresponding simulated curves for the real and imaginary parts of the input impedance are shown in Fig. 6. It can be observed that the radius for both the graphene-ink cylinders and the graphene-powder cylinder should be set to a moderate value to achieve good impedance matching. This is partly attributed to the hybrid copper-graphene structure and the conductivity-based impedance properties.

E. E-FIELD DISTRIBUTIONS

The simulated E-field distributions in the yz cross-section plane of the proposed antenna are illustrated in Fig. 7. The observed frequencies are: 2 GHz, 10 GHz, and 18 GHz, respectively. It can be seen that the E-field distributions are similar to those of a folded monopole and differ in the lower (<10 GHz) and higher (>10 GHz) bands. The two types of E-field distributions correspond to two different radiation

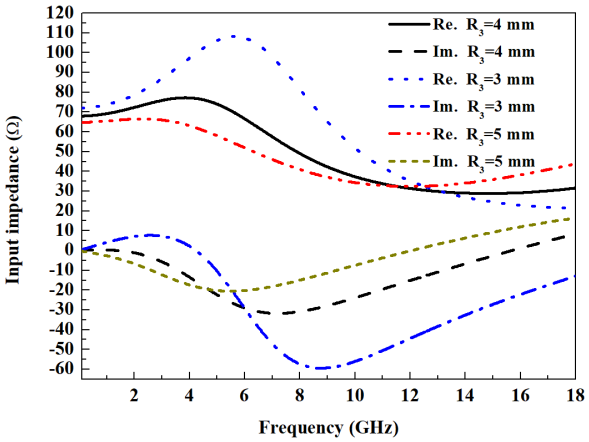

FIGURE 6: Effect of varying the radius of the graphene-powder cylinder on the antenna input impedance.

modes (modes #1 and #2) across a wide bandwidth. These modes combine to generate a super-wideband bandwidth with a monopole-like radiation pattern. In the lower band, the radiating E-fields mainly originate from the top-hat copper disc, the graphene-ink cylinders, and the graphene-powder cylinder. In the higher band, the radiating E-fields mainly originate from certain sections of the graphene-ink cylinders. Notably, the radiating direction of the E-fields from the graphene-ink cylinders is reversed between the lower and higher bands. This is partly attributed to the hybrid copper-graphene properties, as the frequency response of the antenna below 10 GHz is primarily determined by the contact between the graphene ink and copper. Meanwhile, frequencies above 10 GHz are mainly influenced by the contact among the graphene powder, the graphene ink and copper [28].

III. EXPERIMENTS AND ANTENNA PERFORMANCE

The designed antenna was fabricated and assembled to produce several prototypes for comparison and experiments. A photograph of the prototypes is depicted in Fig. 8. Notably, for the fabricated antenna, the conductivity of the graphene-powder and the graphene-ink samples, made from multilayer nanographene, are approximately 100000 S/m. The average thickness of the graphene is 1 to 3 nm, and the number of layers in the multilayer graphene is 2 to 5. The reflection coefficients ($|S_{11}|$) of the antenna were measured using an Agilent E8364B PNA vector network analyzer. The radiation patterns were measured in a microwave far-field anechoic chamber.

A. REFLECTION COEFFICIENTS

The simulated $|S_{11}|$ of the proposed antenna is presented in Fig. 9. Additionally, the measured $|S_{11}|$ for two fabricated antenna prototypes—one with conducting wires that underwent DC voltage excitation once (the proposed antenna in fabrication) and the other with no conducting wires and no DC voltage excitation—are contrasted in Fig. 9. It can be observed that for the proposed antenna, its simulated

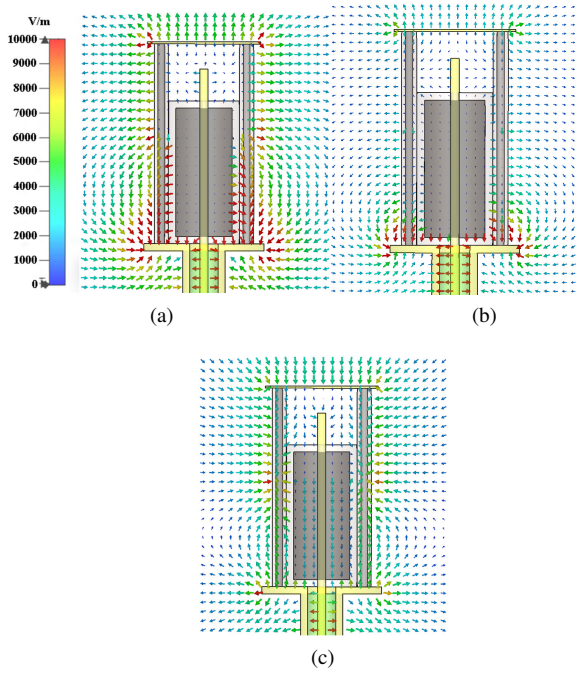

FIGURE 7: Simulated E-field distributions of the proposed antenna at different frequencies: (a) 2 GHz, (b) 10 GHz, (c) 18 GHz.

impedance bandwidth spans 0.1-18 GHz with $|S_{11}|$ <-6 dB [13]. For the measured $|S_{11}|$ of the proposed antenna, its impedance bandwidth spans 0.114-0.202 GHz and 0.34-18 GHz with $|S_{11}|$ <-6 dB. The two measured results indicate that by applying DC voltage excitation once and loading the conducting wires, a degraded $|S_{11}|$ curve can be obtained. This is mainly due to the generated graphene doping, which could improve impedance matching and extend the operating bandwidth toward lower frequencies [23]. The discrepancy between the simulated and measured results can mainly be attributed to fabrication errors and environmental influences, such as the difference between the simulated graphene materials and the practical graphene samples, as well as environmental contamination that could lead to inaccurate conductivity properties of graphene. It should be mentioned that in the simulation, at a fixed frequency, lowering the dielectric constant of the graphene-powder cylinder shifts the corresponding operating band toward higher frequencies. Conversely, increasing the conductivity of the graphene-powder cylinder shifts the corresponding operating band toward lower frequencies.

B. RADIATION PERFORMANCE

The simulated and measured normalized radiation patterns of the proposed antenna are depicted in Fig. 10. The radiation patterns exhibit typical monopole-like characteristics. The measured radiation patterns are asymmetric in the E-plane, primarily attributed to the asymmetrical assembly

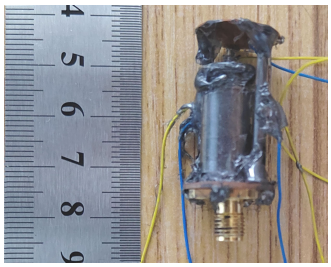

FIGURE 8: Fabricated prototype of the proposed antenna.

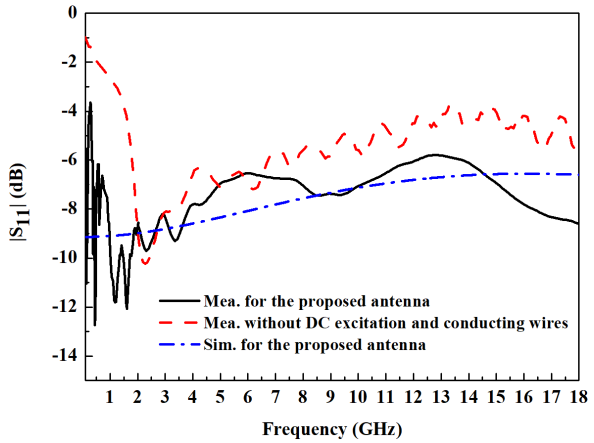

FIGURE 9: Simulated and measured reflection coefficients ($|S_{11}|$) of the proposed antenna. The $|S_{11}|$ measurement for the proposed antenna was conducted using the fabricated antenna embedded with conducting wires and applying DC excitation once.

during the antenna fabrication process. For example, the conducting wires connected at the excitation point 1 are slightly displaced from the center of the top-hat copper disc. In the lower band at 0.13 GHz, the measured E-plane radiation pattern is far away "8"-shape. Additionally, as the frequency increases, the measured radiation patterns exhibit more pronounced monopole-like characteristics. This is partly due to the dominance of radiation mode #1 in the lower band, with some radiation originating from the top-hat copper disc. The simulated antenna gains reach up to: -0.50 dBi (at 0.13 GHz), 3.14 dBi (at 2 GHz), -1.70 dBi (at 10 GHz), and 0.00 dBi (at 18 GHz). The measured antenna gains reach up to: 3.50 dBi (at 0.13 GHz), -0.87 dBi (at 2 GHz), -1.17 dBi (at 10 GHz), and -3.75 dBi (at 18 GHz). The simulated and measured antenna gains versus frequency curves are detailed in Fig. 11. The measured antenna peak gains range from -3.75-3.50 dBi. It should be noted that at a frequency of 0.13 GHz, the embedded conducting wires can enhance the antenna gain, resulting in a measured gain of 3.50 dBi compared to a simulated gain of -0.50 dBi. The simulated radiation efficiency of the proposed antenna ranges from approximately 43% to 87% across the super-wideband bandwidth. The differences between the simulation and the measurement are partly attributed to the challenging fabri-

cation techniques associated with using graphene, such as difficulties in controlling graphene properties and variations in graphene-based material properties.

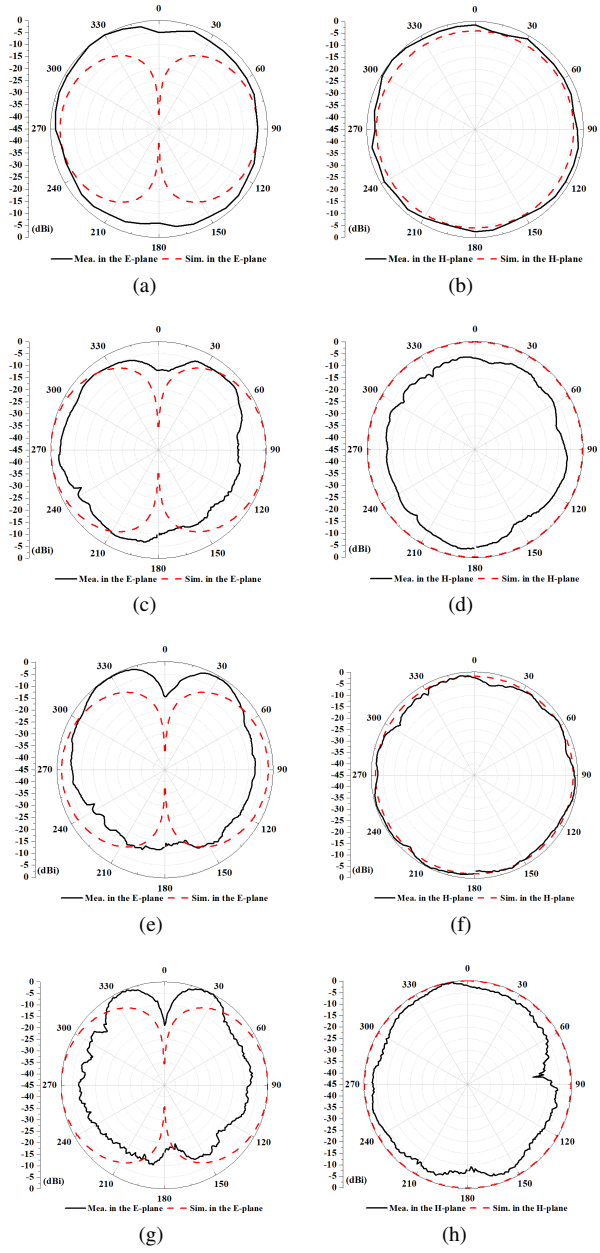

FIGURE 10: Simulated and measured normalized radiation patterns of the proposed antenna at different frequencies: (a) E-plane at 0.13 GHz, (b) H-plane at 0.13 GHz, (c) E-plane at 2 GHz, (d) H-plane at 2 GHz, (e) E-plane at 10 GHz, (f) H-plane at 10 GHz, (g) E-plane at 18 GHz, (h) H-plane at 18 GHz.

C. PERFORMANCE COMPARISON

The proposed antenna is compared to other similar antennas, including both non-graphene-based ultra-wideband antennas and graphene-based ultra-wideband antennas. The results are presented in Table 1. It is evident that the proposed antenna has advantages in terms of size and bandwidth, utilizing a hybrid configuration that incorporates both copper and graphene-based materials for the radiating elements.

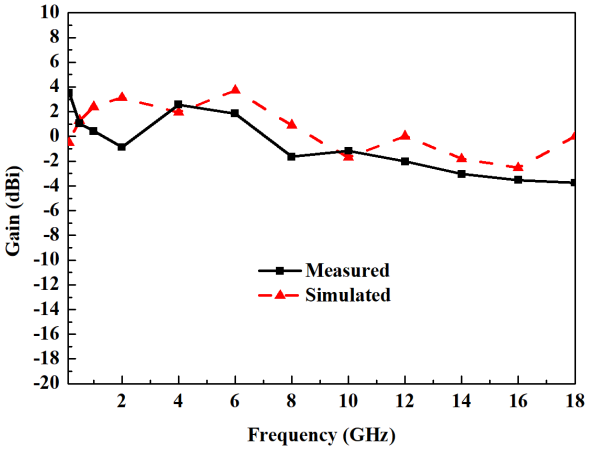

FIGURE 11: Simulated and measured antenna gain versus frequency.

IV. CONCLUSION

A super-wideband miniaturized graphene-based folded monopole antenna is proposed, fabricated, and measured. Simulation and measurement research have been conducted to determine the antenna configuration and investigate the underlying working principles. Although there are some discrepancies between the simulated and measured results, these could be improved by using more accurate fabrication techniques and suitable graphene materials. Compared to existing graphene-based antennas, the proposed antenna has the advantages of extending a super-wideband bandwidth toward lower frequencies while maintaining a very small electrical size. This is achieved through a hybrid design that combines both copper and graphene-based materials for the radiating elements.

ACKNOWLEDGMENT

This work was supported in part by the Research Foundation of Education Bureau of Hunan Province, China contract number 23B0164.

REFERENCES

[1] R. C. Hansen, 'Fundamental limitations in antennas," Proceedings of the IEEE , vol. 69, no. 2, pp. 170-182, Feb. 1981.
[2] S. K. Palaniswamy, M. Kanagasabai,S. Arun Kumar, M. G. N. Alsath, S. Velan, and J. K. Pakkathillam, "Super wideband printed monopole antenna for ultra wideband applications," Int. J. Microw. Wirel. Technol., vol. 9, pp. 133–141, Feb. 2017.
[3] E. A. Aydın, "3D-printed graphene-based bow-tie microstrip antenna design and analysis for ultra-wideband applications," Polym., vol. 13, Nov. 2021.
[4] Y. K. Kim, Y. Lee, K. –Y. Shin, and J. Jang, "Highly omnidirectional and frequency tunable multilayer graphene-based monopole patch antennas," J. Mater. Chem. C, vol. 7, no. 26, pp. 7915-7921, 2019.

TABLE 1: Performance comparison with other super-wideband antennas primarily based on measurement.

Ref.	Dimensions	Lower band edge frequency	Upper band edge frequency	Peak gain (dBi)	Simulated radiation efficiency (%)	Antenna configurations, materials used for radiating elements
[3]	$0.586\lambda_L \times 0.293\lambda_L \times 0.011\lambda_L$	2 GHz	20 GHz	9.1	N/A	Bow-tie microstrip antenna, graphene composite filament
[14]	$0.213\lambda_L \times 0.106\lambda_L \times 0.053\lambda_L$	2 GHz	40 GHz	12.3	89.8-95.5	Fractal dielectric resonator antenna (DRA), dielectric
[31]	$0.440\lambda_L \times 0.253\lambda_L \times 0.324\lambda_L$	500 MHz	50 GHz	16.1	35-84	Double ridged guide horn (DRGH), aluminium and copper
[32]	$0.060\lambda_L \times 0.060\lambda_L \times 0.037\lambda_L$	100 MHz	6.75 GHz	N/A	26-50	Fractal monopole antenna, graphene-based material
[33]	$0.033\lambda_L \times 0.033\lambda_L \times 0.023\lambda_L$	20 MHz	6 GHz	8.13	40-90	Planar monopole antenna, copper
[34]	$0.325\lambda_L \times 0.325\lambda_L \times 0.003\lambda_L$	1.25 GHz	18 GHz	6.3	>90	Log-periodic toothed antenna, copper
Proposed antenna	$0.006\lambda_L \times 0.006\lambda_L \times 0.011\lambda_L$	114 MHz	18 GHz	3.5	43-87	Monopole antenna, copper and graphene-based materials

[5] S. J. Chen, C. Fumeaux, T. T. Tung, and D. Losic, "High-efficiency microwave graphene antenna," IEEE International Symposium on Antennas and Propagation and USNC/URSI National Radio Science Meeting , San Diego, CA, USA, Jul. 09-14, 2017.

[6] V. Slegeryte, D. Belova-Ploniene, A. Katkevicius, and D. Plonis, "Microwave devices with graphene layers: A review," Proc. IEEE Microw. Theory Tech. Wirel. Commun., pp. 87-92, Oct. 2019.

[7] S. N. H. Sadon, M. H. Jamaluddin, A. Althuwayb, and B. Alali, "A review: The influence of graphene material integration in antenna characteristics in the presence of bias for fifth and sixth generation wireless communication application," Nano Commun. Netw., vol. 39, Mar. 2024.

[8] X. Chen, X. Liu, S. Li, W. Wang, D. Wei, Y. Wu, and Z. Liu, "Tunable wideband slot antennas based on printable graphene inks," Nanoscale, vol. 12, no. 20, pp. 10949-10955, May 2020.

[9] I. Ibanez-Labiano and A. Alomainy, "Hybrid metal-graphene ultra-wideband antenna," International Conference on UK-China Emerging Technologies, Glasgow, United kingdom, Aug. 20-21, 2020.

[10] S. Kosuga, R. Suga, T. Watanabe, O. Hashimoto, and S. Koh, "Characterization of contact properties at interface between metal and graphene up to 15 GHz," Eng. Rep., vol. 3, no. 5, May 2021.

[11] Flemish J., Haupt R. L., "Microstrip patch with adaptive conductivity," IEEE Antennas Propag. Soc. AP S Int. Symp., Honolulu, HI, United states, Jun. 10-15, 2007.

[12] D. Guha and Y. M. M. Antar, "Four-element cylindrical dielectric resonator antenna for wideband monopole-like radiation," IEEE Trans. Antennas Propag., vol. 54, pp. 2657–2662, 2006.

[13] L. Xing, Y. Huang, Q. Xu, and S. Alja'afreh , "A wideband hybrid water antenna with an F-shaped monopole," IEEE Access, vol. 3, pp. 1179-1187, Jul. 2015.

[14] A. Azari, A. Ismail, A, and F. Hashim, " A new super wideband fractal monopole-dielectric resonator antenna," IEEE Antennas Wirel. Propag. Lett., vol. 12, pp. 1014-1016, Aug. 2013.

[15] H. Li, Z. Zhou, Y. He, W. Sun, Y. Li, I. Liberal, and N. Engheta, "Geometry-independent antenna based on epsilon-near-zero medium," Nat. Commun., vol. 13, Jun. 2022.

[16] Z. -G. Liu; M. –Y. Geng, H. Chen, A. –Q. Zhang, and W. -B. Lu, "A perspective on the recent progress of graphene in microwave applications: problems, challenges and opportunities," IEEE Microwave Mag., vol. 24, no. 6, pp. 40-53, Jun. 2023.

[17] J. Li, B. Wu, J. Zhou, C. Fan, Y. Liu, "Impedance regulation of graphene loaded branch for frequency reconfigurable antenna with enhanced radiation efficiency," IEEE Antennas Wirel. Propag. Lett., vol. 23, no. 3, pp. 1065-1069, Mar. 2024.

[18] B. Zheng, X. Li, X. Rao, and N. Li, "Multi-beam conformal array antenna based on highly conductive graphene films for 5G micro base station applications," Sensors, vol. 22, no. 24, Dec. 2022.

[19] R. Fang, R. Song, X. Zhao, Z. Wang, W. Qian, and D. He, "Compact and low-profile UWB antenna based on graphene-assembled films for wearable applications," Sensors, vol. 20, no.9, may 2020.

[20] M. Yasir, P. Savi, S. Bistarelli, A. Cataldo, M. Bozzi, L. Perregrini, and S. Bellucci, "A planar antenna with voltage-controlled frequency tuning based on few-layer graphene," IEEE Antennas Wirel. Propag. Lett., vol. 16, pp. 2380-2383, Jun. 2017.

[21] W. Wang, C. Ma, X. Zhang, J. Shen, N. Hanagata, J. Huangfu, and M. Xu, "High-performance printable 2.4 GHz graphene-based antenna using water-transferring technology," Sci. Technol. Adv. Mater., vol. 20, pp. 870–875, Aug. 2019.

[22] X. Du, I. Skachko, A. Barker, and E. Y. Andrei, "Approaching ballistic transport in suspended grapheme," Nat. Nanotechnol., vol. 3, pp. 491–495, Jul. 2008.

[23] S. Lepak-Kuc, K. Z. Milowska, S. Boncel, M. Szybowicz, A. Dychalska, I. Jozwik, K. K. Koziol, M. Jakubowska, and A. Lekawa-Raus, "Highly conductive doped hybrid carbon nanotube–graphene wires," ACS Appl. Mater. Interfaces, vol. 11, pp. 33207–33220, Sep. 2019.

[24] P. Callaghan and J. C. Batchelor, "Dual-band pin-patch antenna for Wi-Fi applications," IEEE Antennas Wirel. Propag. Lett., vol. 7, pp. 757–760, Aug. 2008.

[25] S. N. H. SaDon, M. H. Jamaluddin, M. R. Kamarudin, F. Ahmad, Y. Yamada, K. Kamardin, and I. H. Idris, "Analysis of graphene antenna properties for 5G applications," Sensors, vol. 19, no. 22, Nov. 2019.

[26] V. M. Pereira, L. G. Hardt, D. G. Fantineli, M. V. T. Heckler, and L. E. G. Armas, "Characterization of dielectric properties of graphene and graphite using the resonant cavity in 5G test band," J. Microw. Optoelectron. Electromagn. Appl., vol. 22, no. 1, pp. 63-76, Mar. 2023.

[27] V. Rumsey, "Frequency independent antennas," 1958 IRE International Convention Record, New York, NY, USA, Mar. 21-25, 1966.

[28] D. –Y. Jeon, K. Joo Lee, M. Kim, D. C. Kim, H. -J. Chung, Y. -S. Woo, and S. Seo, "Radio-frequency electrical characteristics of single layer grapheme," Jpn. J. Appl. Phys., vol. 48, pp. 0916011–0916013, Sep. 2009.

[29] R. K. Chaudhary, K. V. Srivastava, and A. Biswas, "An Investigation on three element multilayer cylindrical dielectric resonator antenna excited by a coaxial probe for wideband applications," IEEE Asia-Pac Conf Appl Electromagn, Port Dickson, Malaysia, Nov. 09-11, 2010.

[30] M. Kouroublakis, N. L.Tsitsas, and G. Fikioris, "Shielding effectiveness of magnetostatically-biased anisotropic graphene by the method of auxiliary sources with a surface current boundary condition," IEEE Trans. Antennas Propag., vol. 71, no. 8, pp. 6830-6838, Aug. 2023.

[31] B. Jacobs, J. W. Odendaal, and J. Joubert, "Wideband 0.5–50 GHz double-ridged guide horn antenna using coaxial-to-ridge waveguide launcher," IET Microwaves Antennas Propag., pp. 1-18, Nov. 2023.

[32] W. Clower, M. J. Hartmann, J. B. Joffrion, and C. G. Wilson, "Additive manufactured graphene composite Sierpinski gasket tetrahedral antenna for wideband multi-frequency applications," Addit. Manuf., vol. 32, Mar. 2020.

[33] Y. Zhang, X. Chen, J. Yao, J. Yang, Z. Mao, and Y. Hua, "A compact ultra-wideband receiving antenna for monitoring applications," Microwave Opt. Technol. Lett., vol. 64, no. 1, pp. 142-148, Jan. 2022.

[34] D. Kim, C. Y. Park, and Y. J. Yoon, "Miniaturized four-arm log-periodic toothed antenna with wide bandwidth," IEEE Antennas Wirel. Propag. Lett., vol. 21, no. 4, pp. 745-749, Apr. 2022.